Int. J. Electrochem. Sci., 8 **(2013)** 9692 - 9703

International Journal of
ELECTROCHEMICAL
SCIENCE
www.electrochemsci.org

Layer-by-layer Assembled Sandwich-Like Carbon Nanotubes/Graphene Oxide Composite as High-Performance Electrodes for Lithium-Ion Batteries

Song-Can Wang, Juan Yang, Xiang-Yang Zhou[*]*, Jie Li*

School of Metallurgy and Environment, Central South University, Changsha 410083, China
[*]E-mail: zxy13908482918@163.com

Received: 15 May 2013 / *Accepted:* 9 June 2013 / *Published:* 1 July 2013

Carbon nanotubes/graphene oxide (CNT/GO) composite with a sandwich-like structure was fabricated by a layer-by-layer (LBL) assembled method. Transmission electron microscopy (TEM) and field emission scanning electron microscopy (FESEM) revealed that the open-ended carbon nanotubes constructed network architecture with well-developed nanopores between the graphene oxide sheets, and formed a laminated sandwich-like film. As an anode material for lithium ion batteries, the composite delivered an initial reversible capacity of 1093 mAh g^{-1} at a current density of 100 mA g^{-1} and remained a reversible capacity of 850 mAh g^{-1} at the 60th cycle. In addition, the composite exhibited high rate capability. Such enhanced lithium storage performance of the composite could be ascribed to the special sandwich-like structure which could provide more sites for Li^+ storage and facilitate lithium ion movement.

Keywords: carbon nanotubes/graphene oxide composite; sandwich-like structure; layer-by-layer assembly; lithium ion batteries

1. INTRODUCTION

Lithium ion batteries (LIBs) are one of the most important energy storage devices used in electric vehicles, cell phones, laptops and other portable devices. With the prosperity of the electric vehicle industry, the next generation of LIBs tends to possess both high gravimetric energy and power capability [1]. Nevertheless, the present commercialized graphitic anode obviously cannot meet this demand due to its relatively lower specific capacity (372 mAh g^{-1}) and poor rate performance [2, 3]. Recently, numerous investigations have proved that graphene nanosheets (GNS) is one of the promising materials for LIB anodes due to their outstanding electrochemical and mechanical properties

such as high electrical conductivity, large specific surface area, and mechanical robustness [4-6]. However, GNS tends to re-stack, dramatically reducing available surface and thus reducing effective capacity of GNS to store energy [7, 8]. In order to tackle this problem, one of the effective approaches is to introduce nanospacers between the graphene sheets. Owing to their synergic effect, CNT can be used as one the most effective spacers to separate the graphene sheets, boosting their specific surface area to enhance their energy storage capacity [9-11]. Yoo et al. [12] reported a reversible capacity of 730 mAh g^{-1} for GNS-CNT mixture at a current density of 50 mA g^{-1}. Recently, Chen et al. [13] reported GNS-CNT composite fabricated by microwave-assisted reduction of graphene oxide in CNT suspension, delivered an initial reversible capacity of 682 mAh g^{-1} and a reversible capacity of 298 mAh g^{-1} after 50 cycles at a current density of 50 mA g^{-1}. Chen et al. [14] synthesized the GNS-CNT film via vacuum filtration, exhibiting good electrochemical performance with a reversible capacity of 618 mAh g^{-1} in the first cycle, 485 mAh g^{-1} in the 100th cycle with a high Coulomb efficiency of 98.5% at a current density of 74.4 mA g^{-1}.

Herein, we exploited LBL technique to assemble sandwich-like CNT/GO composite as anodes for LIBs. The ratio of the CNTs and GO in the as-prepared films could be controlled precisely and the electrodes could be fabricated directly without any binding agent. TEM and FESEM illustrated that the CNTs as spacers distributing between the GO sheets homogeneously enabled the direct formation of porous, all-carbon nanostructures with high surface area. Galvanostatic charge-discharge tests and cyclic voltammetry measurements showed that these CNT/GO thin films exhibited high specific capacity, excellent rate capability and little capacity degradation during long cycle operation.

2. EXPERIMENTAL

2.1. Preparation of GO solution

Natural graphite (Nanjing, China) was used for the preparation of GO via a modified Hummers' method [15]. Graphite powders were first oxidized by reacting them with the concentrated sulfuric acid. The reaction vessel was immersed in an ice bath, and potassium permanganate was added slowly, keeping the reacting temperature around 0 °C. The reaction was allowed to go on for 24 h to fully oxidize graphite into graphite oxide. The graphite oxide was thoroughly rinsed and filtered by diluted hydrochloric acid and deionized water until pH=7 to remove metal ions. GO solution was then obtained by exfoliated graphite oxide suspension through ultrasonication for 1 h.

2.2. Preparation of amine functionalized CNT solution

Multi-wall carbon nanotubes (CNTs) synthesized by conventional CVD method were purchased from XFNANO (95% purity, length 1-5 μm, outer diameter 15-5 nm). CNTs were refluxed in concentrated H_2SO_4/HNO_3 (3/1 v/v, 96% and 70%, respectively) at 70 °C to grow some oxygenized functional groups on their surface, and then washed with deionized water until pH=7 using nylon membrane filter (0.22 μm). After drying at 80 °C for 24 h, the oxygen functionalized CNT powder was

chlorinated by refluxing for 24 h with $SOCl_2$ (Henan Kaifeng Chemical Co. Ltd.) at 70 °C. $NH_2(CH_2)_2NH_2$ (Nanjing Jinyue Chemical Co. Ltd.) was then added with dehydrated toluene (Wanxing Chemical Co. Ltd.) as the solvent when the redundancy of $SOCl_2$ was evaporated. The reaction was carried on for 24 h at the temperature of 70 °C. After washing with ethanol and deionized water several times, amine functionalized CNT (CNT-NH_2) powder was obtained from drying at 80 °C in vacuum for 24 h. A certain amount of as-prepared CNT powder was dispersed in deionized water by ultrasonication for 1 h to produce CNT-NH_2 solution.

2.3. LBL Assembly of CNT/GO Electrodes

Copper foils were exposed to a mixture H_2SO_4:H_2O_2=70:30, v/v, for 30 s and carefully washed with deionized water prior to use. For self-assembly the pretreated copper foils were immersed into a CNT-NH_2 solution for 30 min, followed by thorough rinsing with deionized water and drying under a nitrogen flow. Next, the CNT-NH_2-coated copper foil was immersed into the appropriate aqueous GO dispersion for 30 min, rinsed, and dried. This procedure produced a sandwich layer of CNT-NH_2 and GO on a copper foil. Subsequent layers were self-assembled analogously. The as-prepared samples were denoted as LBL-CNT/GO.

2.4. Preparation of GNS Electrodes

As for comparison, a certain amount of GO solution was reduced by hydrazine hydrate at 95 °C for 24 h. After washing with ethanol and deionized water several times, GNS powder was obtained from drying at 80 °C in vacuum for 24 h. The GNS powder was then mixed with polyvinylidene fluoride (PVDF, 8:2 mass ratio) in N-methylpyrrolidone (NMP). The slurry thus obtained was coated onto copper foils and dried at 120 °C in vacuum to form GNS electrodes.

2.5. Characterization

The surface morphology of both the CNT-NH_2 and GO samples was characterized by using a transmission electron microscope (TEM, JEM-2100). A field emission scanning electron microscopy (FESEM, JASM-6200) was further employed for characterization of the microstructure of LBL-CNT/GO samples. The Fourier transform infrared spectroscopy (FTIR) spectra of the samples were tested on a Nicolet 6700 Fourier transform infrared spectrometer.

2.6. Electrochemical measurements

Electrochemical properties were performed in button cells at room temperature with metallic lithium as the auxiliary and reference electrode. Before cell assembly in an Ar-filled glove box, the electrodes were dried at 120 °C overnight in order to remove traces of water and solvent. Polypropylene membrane (Celgard-2400) was used as a separator. The electrolyte consisted of 1 M

$LiPF_6$ in ethylene carbonate and dimethyl carbonate (EC:DMC 1:1 by w/w). The cells were charged and discharged at different rates ranging from 0.1 A g^{-1} to 4 A g^{-1} between 0.01 and 3 V versus Li/Li^+ on LAND CT-2001A (Wuhan Jinnuo Electron Co. Ltd.). Cyclic voltammetry (CV) was carried out on electrochemical analyzers PAR 2273A (PerkinElmer Inc.). Charge always refers to lithiation, while discharge presents delithiation. Specific capacity values (mAh g^{-1}) are obtained considering only the active material mass of the electrodes.

3. RESULTS AND DISCUSSION

3.1. Morphology and structure characterization

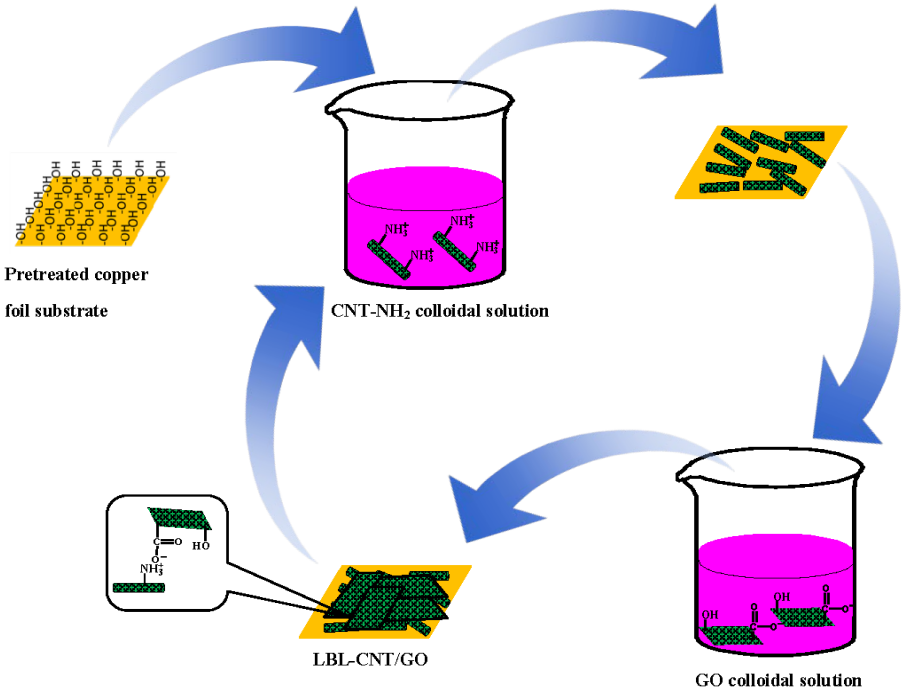

Figure 1. Schematic illustration of the LBL assembly.

The assembly process of LBL-CNT/GO electrodes is shown in Fig. 1. The TEM images of GO and CNT-NH_2 are shown in Fig. 2a and b, revealing a curled morphology consisting of a translucent wrinkled paper-like structure and the short, open-ended pipe structure, respectively. As reported in reference [16] that positively charged CNT-NH_2 and negatively charged GO colloidal dispersions are both very stable in the pH range of 1-4. The GO sheets were sequentially built up on the copper foils in alternation with CNT-NH_2 via electrostatic interactions [17, 18]. FESEM images of 1-layer and 2-layer films are shown in Fig 2c-d. Fig. 2c shows that the individual CNTs are evenly distributed throughout the copper foil, forming a homogeneous network CNT layer. The microstructure of the 2-layer shown in Fig. 2d illustrates an adsorbed monolayer of GO sheets on top of a monolayer of CNTs, where GO sheets stretch on the copper foil steadily via electrostatic interactions with CNTs, and the electrostatic

repulsion of the functional groups grafted on the edge of the GO sheets guarantee the GO films to keep monolayer morphology without any aggregation [19].

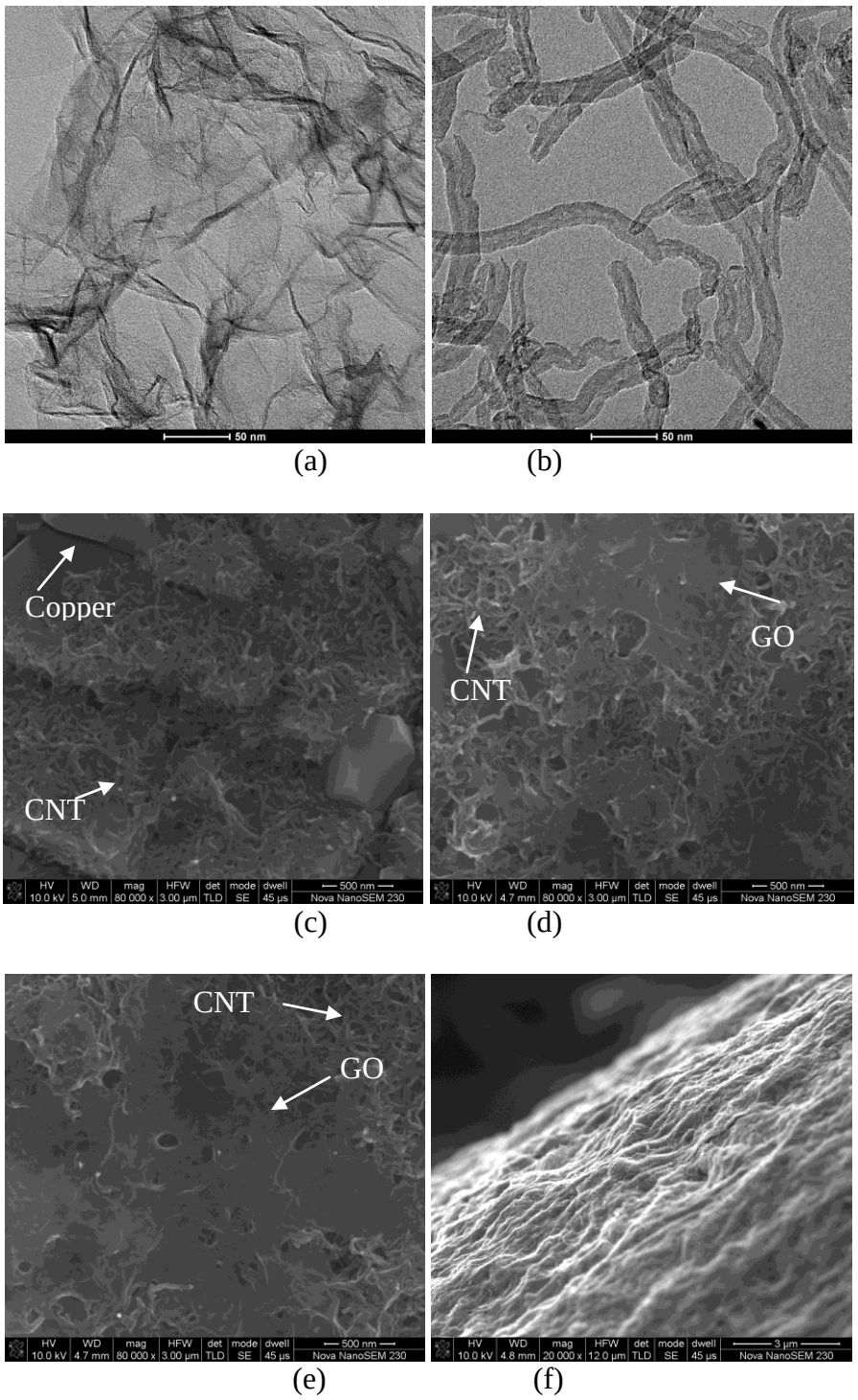

Figure 2 .TEM and FESEM images of GO sheets, CNT-NH_2, and LBL-CNT/GO films: TEM images of (a) GO sheet, and (b) CNT-NH_2; FESEM images of (c) 1-layer of CNT-NH_2 film and (d) 2-layer of CNT and GO films (1 bottom layer of CNT-NH_2 and 1 top layer of GO) on copper foils, (e) top and (f) cross-sectional FESEM images of 20-layer of LBL-CNT/GO film.

The LBL-CNT/GO films were then heat-treated at 150 °C in vacuum for 24 h to increase film mechanical stability and electrical conductivity [20]. The FESEM image of a 20-layer LBL-CNT/GO film in Fig. 2e shows that CNTs and GO sheets are distributed uniformly in-plane, with a transparent GO sheet veiling on the top of the sample. In addition, the FESEM image of the cross-section of the LBL-CNT/GO film in Fig. 2f shows functionalized CNTs interspersed between layers of GO, manifesting a sandwich-like structure. It is proposed that the sandwich structure of the thin film can facilitate ion movement and reduce charge transfer resistance between the GO layers. Moreover, the separated GO layers can significantly enhance the overall electrical conductivity of the thin film due to the good contact with the CNTs and can serve to maintain the stable electrode structure during processing and battery operation.

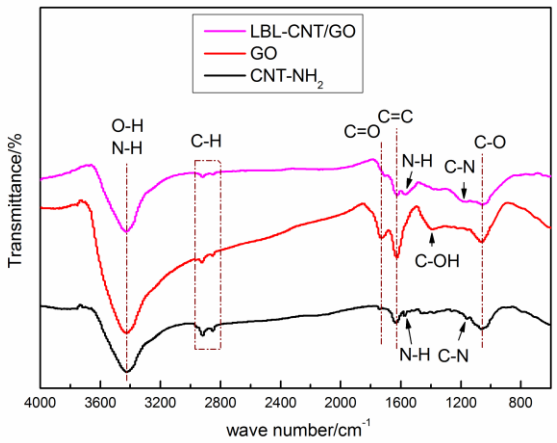

Figure 3. FTIR graphs of LBL-CNT/GO, GO and CNT-NH_2 powders.

The functional groups on the surface and edge of the LBL-CNT/GO， GO and CNT-NH_2 powders are characterized via FTIR and the corresponding FTIR spectra are shown in Fig. 3. All samples show a strong and broad peak around 3430 cm^{-1}, which corresponds to the stretching mode of the O-H group [21]. The bands around 2930 and 2850 cm^{-1} are attributed to the asymmetric CH_2 and symmetric CH_2 stretching of C-H bond and the peak at 1630 cm^{-1} is due to the C=C stretching mode [22, 23]. In GO, the peak at 1730 cm^{-1} is due to C=O (carboxylic acid) stretching vibrations, the peak at 1380 cm^{-1} is due to C-OH stretching vibrations and the peak at 1060 cm^{-1} is due to C-O stretching vibrations [24]. Apart from these similar peaks, two new peaks at 1570 cm^{-1} and 1170 cm^{-1} appear in the FTIR spectra of LBL-CNT/GO and CNT-NH_2, corresponding to the N-H in-plane and C-N bond stretching, respectively [25], which implies that the amino groups have been successfully grafted onto the surface of CNTs and further assembled with GO via electrostatic interactions to form LBL-CNT/GO thin films. In addition, the C=O peaks in LBL-CNT/GO and CNT-NH_2 deviating from 1730 cm^{-1} is caused by the amide carbonyl (-NH-C=O) stretch [26]. It should be mentioned that the peak approximately at 3430 cm^{-1}in the spectra of LBL-CNT/GO and CNT-NH_2 is due to the NH_2 stretch of the amine group overlapped with O-H stretching vibration [27].

3.2. Electrochemical characterization

In order to investigate the potential excellent electrochemical properties of the as-prepared sandwich-like LBL-CNT/GO thin films, half cells were assembled with LBL-CNT/GO thin films as working electrodes. Compared with hydrazine-reduced GNS, the electrochemical properties of LBL-CNT/GO thin films were characterized via charge-discharge test, cyclic voltammetry, and electrochemical impedance spectroscopy measurement.

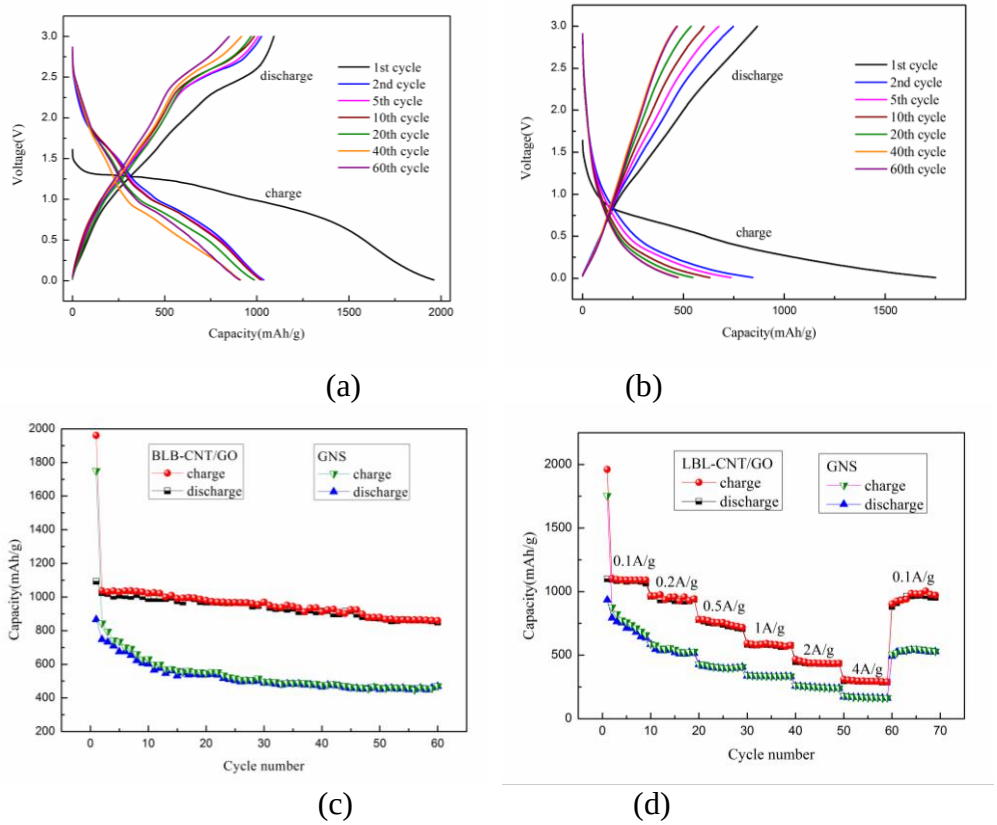

Figure 4. Galvanostatic charge-discharge profiles cycled at the 1st, 2nd, 5th, 10th, 20th, 40th, and 60th cycle of the (a) LBL-CNT/GO, (b) GNS between 3.00 and 0.01 V at a current density of 100 mA g^{-1}. (c) Cycling performance of LBL-CNT/GO and GNS electrodes at a current density of 100 mA g^{-1}; (b) Rate capability of LBL-CNT/GO and GNS electrodes at different current densities from 0.1 to 4 A g^{-1}. (active material mass: 0.1mg for the LBL-CNT/GO electrode while 0.3 mg for the GNS electrode)

Fig. 4a and b present the galvanostatic charge/discharge profiles of the LBL-CNT/GO and GNS at a current density of 100 mA g^{-1} in the 1st, 2nd, 5th, 10th, 20th, 40th, and 60th cycle, respectively. In the first charge curve of the LBL-CNT/GO electrode (Fig. 4a), an extended voltage plateau can be seen around 1.3 V, which is ascribed to the formation of a solid electrolyte interface (SEI) film and the reaction between functional groups and lithium ions according to >C=O + Li^+ + e^- ↔ >C-OLi [28, 29]. By contrast, the extended voltage plateau of GNS in the first charge curve is at about 0.8 V (Fig. 4b) owing to the formation of SEI film. It is noticeable that functional groups can

increase the intercalation voltage plateau to some extent. In the subsequent charge/discharge processes of the LBL-CNT/GO and GNS, the plateaus become higher and more sloping with a lower over potential than those in the first cycle, indicating that the Li^+ insertion reaction is easier. Furthermore, there are two plateaus located at about 1.0 and 2.5 V in the discharge curves of the LBL-CNT/GO electrode, originating from the de-lithiation reaction and reserve reaction between functional groups and lithium ions, respectively. However, in the discharge curves of the GNS electrode, no apparent plateaus can be observed. This implies that the sandwich-like structure and functional groups are conducive to the enhancement of capacity.

The Li^+ storage performance of the LBL-CNT/GO and GNS anode materials for LIBs was characterized by the galvanostatic charge/discharge cycling. At the current density of 100 mA g^{-1} in the voltage window of 0.01-3.00 V, the Li^+ storage capacity versus cycle number is shown in Fig. 4c. The initial charge and discharge capacities for LBL-CNT/GO are 1961 mAh g^{-1} and 1093 mAh g^{-1}, respectively. At the same time for GNS, the initial charge and discharge capacities are 1751 mAh g^{-1} and 867 mAh g^{-1}, respectively. The large initial capacity losses are observed for both LBL-CNT/GO and GNS at the first cycle (with the Coulomb efficiency of 55.7% and 49.5%, respectively), which may be attributed to the lithium ion consumption during the electrolyte decomposition and formation of SEI film around the electrodes with large surface areas. After the formation of a stable SEI film, the capacity of the LBL-CNT/GO decreases very slowly in the following cycles, revealing a discharge capacity of 1025 mAh g^{-1} at the 2nd cycle to 969 mAh g^{-1} at the 20th cycle, then the discharge capacity declines gradually to 850 mAh g^{-1} at the 60th cycle with the Coulomb efficiency of 99%. In contrast, the GNS anode experiences a larger drop, with the discharge capacity of 748 mAh g^{-1} at the 2nd cycle to 538 mAh g^{-1} at the 20th cycle, decreasing steadily to 469 mAh g^{-1} at the 60th cycle with the Coulomb efficiency of 98%. The discharge capacity of LBL-CNT/GO is approximately twice of that of its counterpart GNS after the 15th cycle. This is ascribed to the stable sandwich structure of LBL-CNT/GO (shown in Fig. 2f), where CNTs separate the GO sheets effectively, providing more Li^+ storage locations that naturally lead to an increase in capacity.

Rate capability is another important parameter of LIBs, especially for applications such as hybrid electric vehicles, which are often operated at high charge/discharge rate [30, 31]. The rate performance of a lithium ion battery can strongly depend on the mobility of its electrons and Li^+. The rate capability of LBL-CNT/GO and GNS anode materials at various current densities from 0.1 to 4 A g^{-1} in a voltage window of 0.01-3.00 V at ambient temperature was evaluated (Fig. 4d). In this experiment, cells were cycled at stepped current densities of 0.1 A g^{-1}, 0.2 A g^{-1}, 0.5 A g^{-1}, 1 A g^{-1}, 2 A g^{-1}, 4 A g^{-1} and then back to 0.1 A g^{-1}, 10 cycles for each current densities. As demonstrated in Fig. 5b, the LBL-CNT/GO shows much higher reversible capacities than GNS at all the current densities examined, even at the highest current density of 4 A g^{-1}. Compared with the discharge capacity of the 9th cycle at various current densities, LBL-CNT/GO anode is found to sustain higher capacity retention at 0.2 A g^{-1}, 0.5 A g^{-1}, 1 A g^{-1}, 2 A g^{-1}, and 4 A g^{-1} relative to the capacity at 0.1 A g^{-1} than that of GNS anode. The reversible discharge capacity of LBL-CNT/GO is much larger than that of the GNS, even at the current density of 4 A g^{-1}, LBL-CNT/GO exhibits the reversible discharge capacity of 287 mAh g^{-1}, while GNS only remains 163 mAh g^{-1}. Moreover, when the current density drops back to 0.1 A g^{-1}, the reversible capacities of LBL-CNT/GO and GNS jump to 953 mAh g^{-1} and 528 mAh g^{-}

^{1}, respectively (shown in Fig. 4d). Excepting the initial charge capacities of the two electrodes, the charge capacities at the following cycles are approximately equivalent to the discharge ones, implying the excellent reversibility of energy storage.

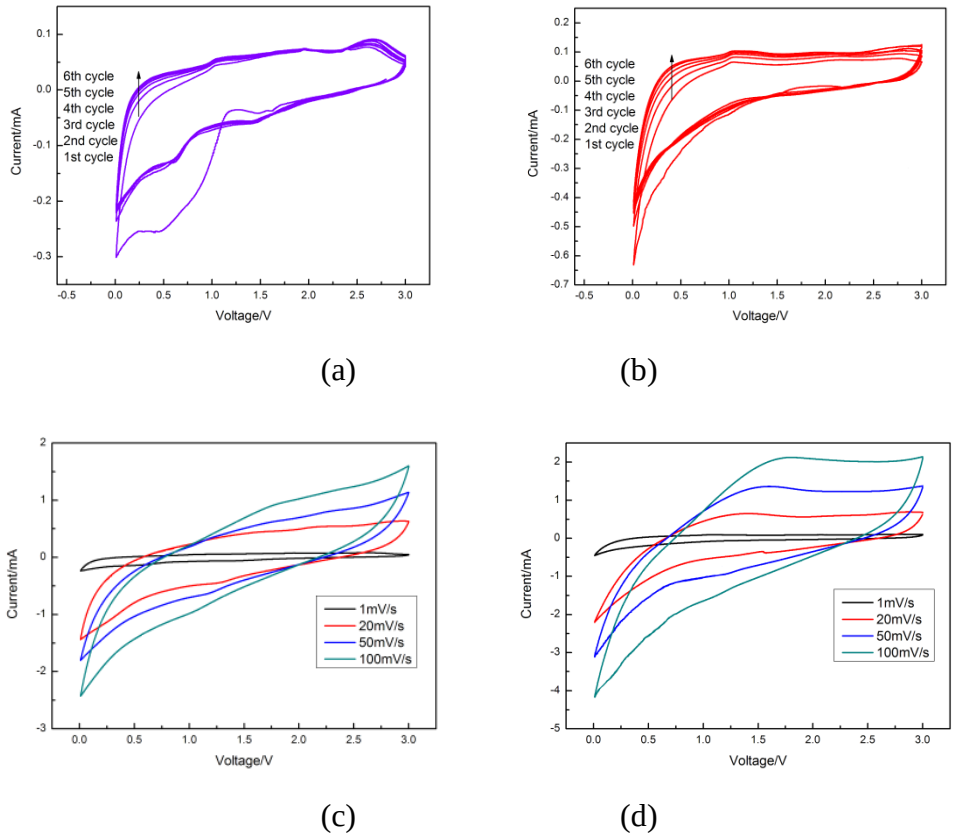

Figure 5. Voltammograms collected at low scan rate (1mV s^{-1}) and high scan rate (100, 50, 20, 1mV s^{-1}) for the LBL-CNT/GO (a, c) and GNS (b, d).

For conventional electrodes, the charge capacities decrease with the increasing of the current density. Li^+ diffusion coefficient inside electrode materials is limited during the processes of Li^+ intercalation/de-intercalation. This might be attributed to the gradient of the Li^+ concentration in anodes during discharge/charge process. The potential drops to the cut-off potential rapidly when anode surface completes the discharge, but the center of the anodes does not complete the discharge process [32, 33], which causes the capacity loss at high current densities. The higher the current density is, the larger the capacity loses. The as-prepared LBL-CNT/GO electrode, however, provides stable transmission paths for Li^+ due to its sandwich-like structure, which decreases the resistance of Li^+ migration, accelerating the speed of Li^+ intercalation/de-intercalation. Therefore, the rate performance of the LBL-CNT/GO electrode has been improved to some extent.

Cyclic voltammetry (CV) experiments were further conducted to evaluate the electrochemical performance of the LBL-CNT/GO and GNS anodes at a scanning rate of 1 mV s^{-1} over the voltage range of 0.01-3.00 V (Fig. 5a and b). Both of the voltammograms in Fig. 5a and b exhibit an imbalance

between the cathodic and anodic charges that vanish or decrease in the second cycle. There are also cathodic peaks in the first cycle that disappear or are drastically modified in the subsequent cycles, which can be interpreted on the basis of electrolyte decomposition and the formation of the stable SEI film [34], conforming to the relatively low coulomb efficiency in the first galvanostatic charge/discharge cycle (shown in Fig. 4c). The cathodic peak close to 0 V is due to the Li^+ intercalation into LBL-CNT/GO and GNS. The observed anodic peaks located at 0.2 V show Li^+ de-intercalation process from anodes. In comparison to GNS, LBL-CNT/GO anode exhibits another two different cathodic peaks at 1.6-1.2 V and 0.7-0.4 V reflecting extra Li^+ storage sites resulting from the anchored CNT-NH_2, which is beneficial to increase the specific capacity.

It can be noticed that all the cathodic and anodic peaks of the LBL-CNT/GO anode are almost keep on the same intensity after the first cycle (shown in Fig. 5a), indicating that LBL-CNT/GO possesses excellent cycle performance. However, the anodic peaks of the GNS anode eyewitness an upward trend during the same period of cycling (shown in Fig. 5b), which means the cycle performance of the LBL-CNT/GO is better than that of the GNS anode. This result is consistent with that of cycling test (Fig. 4c).

In order to investigate the high rate capability of the as-prepared anodes, the LBL-CNT/GO and GNS anodes were further tested at a higher scan rate in the same voltage range. As shown in Fig. 5c and d, when calculating the area of each cycle, reveals that the LBL-CNT/GO has energy densities of 3.07 C g^{-1}, 18.75 C g^{-1}, 22.34 C g^{-1}, and 30.32 C g^{-1} at 1 mV s^{-1}, 20 mV s^{-1}, 50 mV s^{-1} and 100 mV s^{-1}, respectively. When under the same scan rate, the energy densities of GNS are 1.43 C g^{-1}, 7.71 C g^{-1}, 13.61 C g^{-1} and 19.52 C g^{-1}, respectively. It can be suggested that the stable sandwich structure of the LBL-CNT/GO provides much larger specific surface area that behaves better double layer charge/discharge performance as well as the pseudocapacity properties afforded by the functional groups [35]. Therefore, the LBL-CNT/GO anode expresses better rate capability even in high current density (shown in Fig4. d).

To understand the reason for the improved electrochemical lithium storage performance of the LBL-CNT/GO and GNS anodes, electrochemical impedance spectroscopy (EIS) measurements are carried out after the 6th cycle of CV test at a scanning rate of 1 mV s^{-1} over the voltage range of 0.01-3.00 V and their corresponding Nyquist plots are shown in Fig. 6. Both anodes show a straight line in the low-frequency region and a semicircle in the high frequency region. The intersection of the curve with the X-axis represents the internal resistance (IR) which is a key parameter in influencing the charge/discharge rate, as a smaller IR represents a lesser internal loss and a greater charge/discharge rate. As seen from the curves, the IR of the LBL-CNT/GO is lower than that of the GNS, indicating the charge/discharge rate of the LBL-CNT/GO anode is greater. The low-frequency tails in the graph can be compared qualitatively with reference to the mass (mainly of lithium ions) transfer kinetics in the electrode materials [36]. The low-frequency slope angle of the LBL-CNT/GO anode is higher than that of the GNS. The steeper low-frequency tail indicates higher lithium ion conductivity in the electrode materials [37]. As expected, it indicates that the LBL-CNT/GO anode possesses a high electrical conductivity, a rapid charge-transfer process, and good Li-ion kinetics for lithium insertion and extraction.

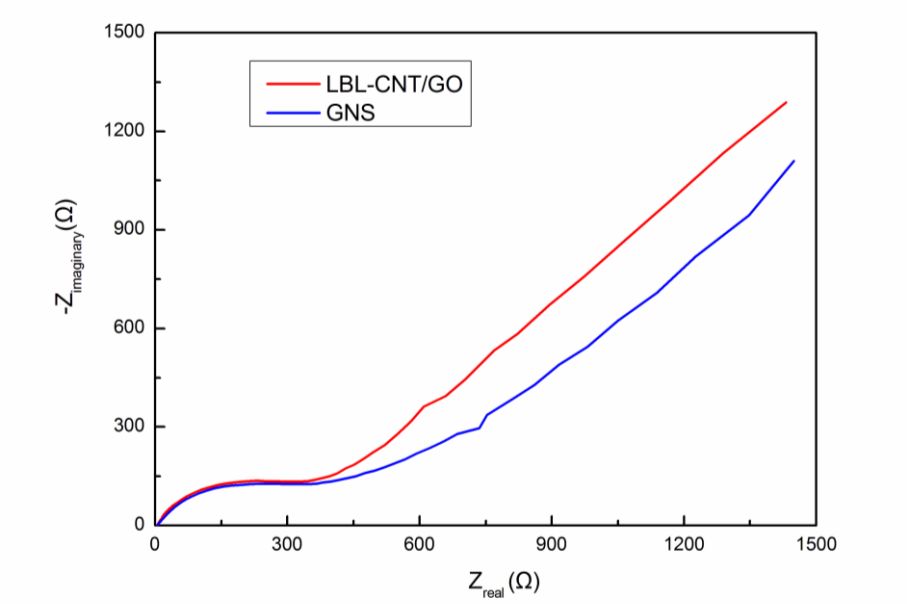

Figure 6. Electrochemical impedance spectroscopy (EIS) measurements: Nyquist plots of the LBL-CNT/GO and GNS anodes. EIS measurements were carried out between 10 kHz and 10 mHz after 6 cycles of CV test at a scaning rate of 1mV s^{-1}.

4. CONCLUSIONS

CNTs are uniformly distributed between the graphene oxide sheets via amide bonds to form a sandwich-like structure via layer by layer assembled method. Such a microstructure provides favorable transport kinetics for both the lithium ions diffusion across the SEI film and the electronic transfer. Consequently, this LBL-CNT/GO anode delivers a large initial reversible capacity of 1093 mAh g^{-1} , and 77.8% of this capacity can be retained after 60 cycles at the current density of 100 mA g^{-1}, which is approximately twice of that of its counterpart GNS anode. When the current density is increased to 4 A g^{-1}, the LBL-CNT/GO anode still exhibits a reversible discharge capacity of 287 mAh g^{-1} and good cycling performance as well. Therefore, LBL-CNT/GO composite with a sandwich-like structure can be a promising candidate of electrode material for application in electrical energy conversion and storage.

ACKNOWLEDGMENTS
This study was supported by the National Natural Science Foundation of China (51274240, 51204209). Moreover, the authors are grateful to Prof. Y.H. Qin and A. Prof. Q.H. Tian for their kind helpful assistance.

References

1. C. Kang, I. Lahiri, R. Baskaran, W. G. Kim, Y. K. Sun, and W. Choi, *J. Power Sources*, 219 (2012) 364.
2. G. X. Wang, X. P. Shen, J. Yao, and J. Park, *Carbon*, 47 (2009) 2049.

3. S. Park, and R. S. Ruoff, *Nat. Nanotechnol*., 4 (2009) 217.
4. N. Zhu, W. Liu, M. Xue, Z. Xie, D. Zhao, M. Zhang, J. Chen, and T. Cao, *Electrochim. Acta*, 55 (2010) 5813.
5. X. H. Rui, M. O. Oo, D. H. Sim, S. C. Raghu, Q. Y. Yan, T. M. Lim, and M. Skyllas-Kazacos, *Electrochim. Acta*, 85 (2012) 175.
6. W. Gao, N. Singh, L. Song, Z. Liu, A. L. M. Reddy, L. Ci, R. Vajtai, Q. Zhang, B. Wei, and P. M. Ajayan, *Nat. Nanotechnol*., 6 (2011) 496.
7. H. W. Tien, Y. L. Huang, S. Y. Yang, J. Y. Wang, and C. C. M. Ma, *Carbon*, 49 (2011) 1550.
8. D. Li, M. B. Müller, S. Gilje, R. B. Kaner, and G. G. Wallace, *Nat. Nanotechnol*., 3 (2008) 101.
9. D. N. Futaba, K. Hata, T. Yamada, T. Hiraoka, Y. Hayamizu, Y. Kakudate, O. Tanaike, H. Hatori, M. Yumura, and S. Iijima, *Nat. Mater*., 5 (2006) 987.
10. G. P. Dai, C. Liu, M. Z. Wang, and H. M. Cheng, *Nano Lett*., 2 (2002) 503.
11. T. Ishihara, A. Kawahara, H. Nishiguchi, M. Yoshio, and Y. Takita, *J. Power Sources* 97&98 (2001) 129.
12. E. J. Yoo, J. Kim, E. Hosono, H. S. Zhou, T. Kudo, and I. Honma, *Nano Lett*., 8 (2008) 2277.
13. T. Q. Chen, L. K. Pan, K. Yu, and Z. Sun, *Solid State Ionics*, 229 (2012) 9.
14. S. Q. Chen, W. Yeoh, Q. Liu, and G. X. Wang, *Carbon*, 50 (2012) 4557.
15. W. S. Hummers, and R. E. Offeman, *J. Am. Chem. Soc*., 80 (1958) 1339.
16. H. R. Byon, S. W. Lee, S. Chen, P. T. Hammond, and Y. Shao-Horn, *Carbon*, 49 (2011) 457.
17. Y. K. Kim, and D. H. Min, *Langmuir*, 25 (2009) 11302.
18. A. K. Sarker and J. D. Hong, *Langmuir*, 28 (2012) 12637.
19. J. Kim, L. J. Cote, and J. X. Huang, *Acc. Chem. Res*., 45 (2012) 1356.
20. S. W. Lee, B. S. Kim, S. Chen, Y. Shao-Horn, and P. T. Hammond, *J. Am. Chem. Soc*., 131 (2009) 671.
21. S. H. Jin, Y. B. Park, and K. H. Yoon, *Compos. Sci. Technol*., 67 (2007) 3434.
22. G. Vuković, A. Marinković, M. Obradović, V. Radmilović, M. Čolić, R. Aleksić, and P. S. Uskoković, *Appl. Surf. Sci*., 255 (2009) 8067.
23. M. S. Ahmed, and S. Jeon, *J. Power Sources*, 218 (2012) 168.
24. L. J. Zhang, X. G. Zhang, L. F. Shen, B. Gao, L. Hao, X. J. Lu, F. Zhang, B. Ding, and C. Z. Yuan, *J. Power Sources* 199 (2012) 395.
25. T. Ramanathan, F. T. Fisher, R. S. Ruoff, and L. C. Brinson, *Chem. Mater*., 17 (2005) 1290.
26. T. Ramanathan, H. Liu, and L. C. Brinson, *J. Polym. Sci., Part B: Polym. Phys*., 43 (2005) 2269.
27. C. T. Hsieh, H. Teng, W. Y. Chen, and Y. S. Cheng, *Carbon*, 48 (2010) 4219.
28. H. C. Shin, M. Liu, B. Sadanadan, and A. M. Rao, *J. Power Sources*, 112 (2002) 216.
29. B. Z. Jang, C. G. Liu, D. Neff, Z. N. Yu, M. C. Wang, W. Xiong, and A. Zhamu, *Nano Lett*., 11 (2011) 3785.
30. K. Kang, Y. S. Meng, J. Bréger, C. P. Grey, and G. Ceder, *Science*, 311 (2006) 977.
31. B. Kang, and G. Ceder, *Nature*, 458 (2009) 190.
32. T. W. Jones, A. P. Lewandowski, and S.W. Donne, *Electrochim. Acta*, 56 (2011) 4996.
33. Y. J. Mai, J. P. Tu, C. D. Gu, and X. L. Wang, *J. Power Sources*, 209 (2012) 1.
34. G. Eda, G. Fanchini, and M. Chhowalla, *Nat. Nanotechnol*., 3 (2008) 270.
35. C. Uthaisar, and V. Barone, *Nano Lett*., 10 (2010) 2838.
36. S. S. Zhang, K. Xu, and T. R. Jow, *Electrochim. Acta*, 49 (2004) 1057.
37. Y. Ma, C. Zhang, G. Ji, and J. Y. Lee, *J. Mater. Chem*., 22 (2012) 7845.